Behavioral maps organize smartphone interactions in the brain

Wenyu Wan[1,2*], K. Richard Ridderinkhof[2], Arko Ghosh[1*]

[1]Cognitive Psychology Unit, Institute of Psychology, Leiden University, The Netherlands

[2]Department of Psychology, University of Amsterdam, The Netherlands

*Corresponding authors:

Wenyu Wan & Arko Ghosh

Institute of Psychology

Leiden University Wassenaarseweg 52

Leiden, 2333 AK, the Netherlands.

Email: w.wan@fsw.leidenuniv.nl [Wenyu Wan]

Email: a.ghosh@fsw.leidenuniv.nl [Arko Ghosh]

Abstract

Smartphones are used for different purposes, with each touchscreen interaction (taps and swipes) shaped by a distinct combination of cognitive, affective, and environmental factors. Given this uniqueness of each interaction, it would seem reasonable to treat one interaction as independent from another. Yet, emerging evidence suggests the opposite: when smartphone interactions are analyzed based on their inter-interaction interval properties, they reveal structured patterns and point to common underlying processes linking distinct interactions. To address the possibility of common neural processes underlying distinct interactions, we recorded EEG signals during hour-long smartphone use sessions spanning various activities (n = 53 participants, accumulating 136,869 taps). We tracked the next-interval property of each interaction in a two-dimensional behavioral map spanning 100 ms to 10 s. Independent component analysis of the EEG signals identified twelve broad neural signal sources. The neural signals time-locked to touchscreen interactions organized into clusters across the behavioral map, with neighboring locations sharing common neural sources and timing patterns. These clusters differed across individuals but were generally more pronounced in the signals preceding the touchscreen interaction than those following it, suggesting individualized neural strategies for planning and executing sequential smartphone interactions. Our findings show that neural processes are systematically organized according to a behavioral map derived from the temporal dynamics of short action sequences. We propose that this organization allows the brain to efficiently allocate neural resources through a low-dimensional representation of real-world behavioral dynamics.

Keywords: smartphone behavior, temporal dynamics, interval statistics, neuro-behavioral clusters

Introduction

Smartphone use is a hallmark of modern human behavior, with each touchscreen interaction serving a unique outcome—whether moving to the next picture in an album or typing a message to a friend. Apart from the distinct behavioral goals, these interactions occur under the influence of various intrinsic and extrinsic factors: from feeling fatigued to adopting different body postures, and from using an app with a colorful layout to viewing an old webpage. Given this complex combination of goals and factors, it would be natural to assume that one touchscreen interaction is simply independent from another. On the other hand, interactions might be linked when driven by common goals or motor sequences. Two distinct lines of evidence support this latter view. First, neural population signals captured using EEG show time-locked averaged signals when thousands of interactions are pooled together (1). When

the interaction-to-interaction variability cancels out through averaging, systematic neural processes emerge, indicating that common time-locked processes are engaged during touchscreen interactions. Second, there is a series of emerging results from the study of intervals between touchscreen interactions. The timing between events shows the same kind of burst-like structure whether one looks at seconds, hours, or days — but this multi-scale pattern is correlated to the sensorimotor limits captured in the sub-second timescales (2). This is akin to how the interval structures in computer servers reflect bandwidth and other resource constraints intrinsic to the computer (3). This idea is further extended in the study of touchscreen next interval dynamics—where the distributions characterize how one interval follows the next—and these distributions reflect aging and neurological disease: as if intrinsic constraints shape the emergent behavioral structures (4–7).

Here we test whether the brain organizes natural behavior using low-dimensional representations of interval transitions, by linking smartphone-derived next-interval statistics to time-resolved EEG dynamics. Rather than treating touches as isolated events, we treat them as samples from an ongoing behavioral dynamic system. This approach to studying smartphone interactions draws inspiration from so-called Poincaré sections and return maps, as widely used to study complex systems (8–10). Our intuition is that intricate cascades of neural and cognitive processes underlie behavioral outputs, resulting in what can be conceptualized as a behavioral flow—a continuous trajectory through different behavioral states. It is difficult to directly study and interpret this flow. The touchscreen offers a lower-dimensional section of this flow, akin to a Poincaré section in dynamical systems—each interaction represents a moment where the flow passes through an observable plane. This section tracks how much time passes between consecutive interactions, i.e., the interval. These intervals can be then used to describe the behavioral system using a map of next-interval properties (11). For instance, a short interval followed immediately by another short interval occupies a different location on this map than a short interval transitioning to a long interval. This return map—termed the joint-interval distribution (JID)—captures the emergent patterns in smartphone interactions. Thus, the JID is simply a 2D map describing how one inter-interaction interval transitions to the next. Remarkably, diverse behaviors occupying neighboring locations on this map show meaningful covariation: multi-day rhythms emerge across clusters of behaviors spanning neighboring locations, and these patterns are impacted by seizures and aging (4, 5, 12). Such patterns, which cut across behavioral domains, suggest that the brain not only is exposed to these statistics but may leverage these low-dimensional emergent patterns to orchestrate its rich behavioral repertoire.

This raises a fundamental question: does the brain merely produce these interval statistics as a by-product of behavior, or does it actively represent this low-dimensional temporal structure?

The patterns revealed by the JID suggest a deeper principle at work in neural organization. A large body of work shows that the brain is sensitive to temporal regularities and exploits them for prediction, perception, and action. Neural systems track transitional probabilities, rhythmic patterns, and higher-order structures in streams of sensory input (13, 14). Critically, these regularities are not merely learned but are continuously exploited to shape ongoing processing. For instance, predictive coding theories propose that cortical circuits generate expectations based on inferred regularities and compare them with incoming sensory signals, minimizing prediction errors through hierarchical message-passing between cortical levels (15, 16). Neurophysiological studies show that such expectations sharpen neural representations, bias attention, and accelerate detection of anticipated events (17). These observations and theories raise the possibility that the brain captures high-dimensional regularities in lower-dimensional representations, which are then proactively deployed to navigate the complexity of the original input structures. This principle may extend beyond perception to the complex structure underlying our actions (18, 19), suggesting a unified framework for understanding behavioral regularities. We propose that the brain might do the same for self-generated action statistics.

Conventional approaches offer clues on how brain activity is tuned to low-dimensional temporal structures. However, these well-explored structures are rather simplistic compared to what is seen in smartphone behaviour and are derived from sensory inputs rather than emerging from actions. In such studies, sensory intervals are used to capture sensory statistics, and one consistent finding is that neural activity is distributed across different brain areas to track these intervals, even when the perceptual task engages only a single modality (20–24). For instance, when monkeys discriminate tactile interval durations, neurons in both somatosensory and prefrontal cortices encode these intervals, despite the task engaging only the tactile modality (25, 26). Another insight is that there is a rough separation of brain processes engaged in sub-second vs. supra-second intervals (27–30). These insights are consistent with the idea that distributed neural processes use lower-dimensional representations of temporal patterns.

We recently tested this idea using tactile stimuli with consecutive intervals spanning 100 ms to 10 s, characterizing the stimulus statistics using the JID framework (31). When evoked EEG signals were analyzed according to next-interval properties, different processing stages showed differential tuning to these properties. Notably, intermediary stages—putatively in the secondary somatosensory cortex—clustered in JID space such that neighboring locations elicited similar neural responses. This supports the idea that next-interval statistics provide a lower-dimensional representation that the brain leverages for information processing.

Compelling evidence for lower-dimensional representations in naturalistic, ongoing behavior is currently lacking. Here, we investigated the neural correlates of the joint-interval distribution emerging from touchscreen interactions during everyday smartphone use. We separated EEG signals time-locked to smartphone touches based on their JID locations, with inter-interaction intervals spanning timescales from ~100 ms to ~100 s. We used data-driven dimensionality reduction to extract prototypical neural signal patterns distributed across the JID such that behaviors with similar next-interval dynamics were linked to similar signals, forming neuro-behavioral clusters. Our analysis was conducted at the individual level, and virtually all individuals showed neuro-behavioral clusters in one or more source-separated EEG signals (Independent Component Analysis). Importantly, clusters exhibited prototypical neural features that peak at distinct stages around the touchscreen event before dissolving, indicating that interval-specific neural representations are transient and time-locked to behavior.

Results

Delineating cortical processes surrounding smartphone interactions based on EEG signal source separation

We first estimated the time window surrounding individual touchscreen interactions that contained extensive neural signals related to the action. Towards this, we simultaneously recorded the smartphone interaction-related movement signals with movement sensors attached to the participants' right thumb and EEG signals (Fig. 1A). The grand-averaged movement signals indicated an onset of kinematic activity ~ 1 s prior to the smartphone interaction and lasting for another ~ 1 s after the interaction (Fig.1B, left panel). Although there were considerable inter-individual differences, there was a consistent downward (towards the screen) pattern of thumb flexion close to the smartphone touchscreen interaction. In the EEG recordings, the electrode placed over the contralateral somatosensory cortex also showed time-constrained ERP signals (Fig. 1B, middle panel). To estimate the temporal span of the scalp-wide signals, we used the global field power (GFP), which revealed a period extending from ~1.4 s prior to the interaction and ~ 1 s thereafter (Fig. 1B, right panel) had the most intensive brain response. In keeping with prior observations, these patterns indicate that the discrete smartphone touchscreen interactions are surrounded by a delineated period of kinematic and neurophysiological activity (32). In the subsequent analysis, we focused on this period (Time period of interest, TOI).

We next separated the putatively distinct brain signal sources captured in the TOI by using independent component analysis (ICA). The analysis at the level of each participant revealed ~7 sources (median) spanning various cortical locations. To pool information across the

population-level, we subsequently grouped these sources (n= 433) according to their putative dipole locations, resulting in 12 typical groups (Fig. 1C). The three most prevalent groups were as follows: group#1 (74 ICs from 47 participants, dipoles centered at MNI coordinates [5,-79,8], occupying the occipital regions, likely corresponding to the visual processing), group#2 (41 ICs from 35 participant, dipoles centered at [-3,-21,22], around cingulate cortex, likely involved in cognitive and motor control and attention regulation), group#3 (42 ICs from 31 participants, dipoles centered at [-32,-16,59], around left central gyrus, likely involved in sensorimotor processing). For the full list of groups, see Supplementary Table 1.

In sum, a range of putatively distinct signal sources were observed surrounding smartphone interactions, implicating processes from motor planning to visual information processing. Our subsequent analysis reveals how these segmented neural signals systematically vary across the JID space.

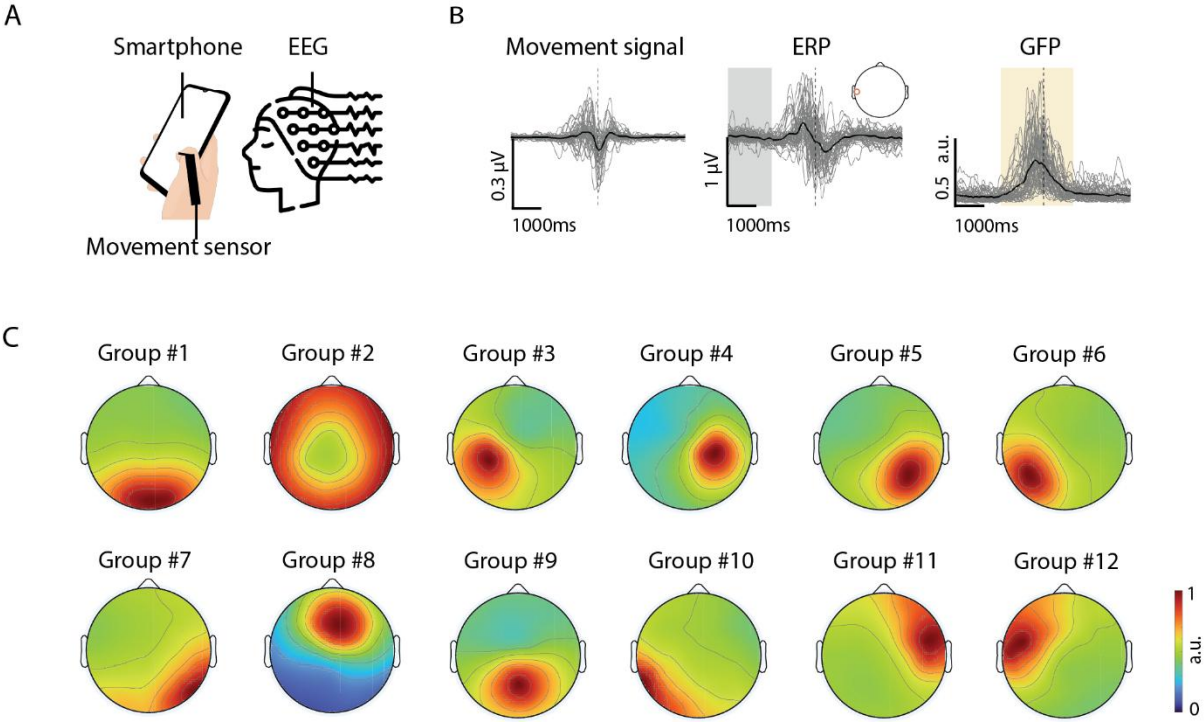

Figure 1. Cortical EEG signals surrounding smartphone touchscreen interactions. (A) Illustration of experimental setup. Timestamps of the smartphone touchscreen event were logged by an App operating in the background on the user's personal smartphone. Right thumb flexion-extension was captured by a movement sensor. Cortical population activity was recorded by using 62-channel scalp EEG. (B) Signals time-locked to smartphone touchscreen interactions. Left: black line indicates the grand-averaged (across participants) movement signals time locked to the smartphone interaction (horizontal dashed line). Individual movement traces are shown in grey. Middle: The grand-averaged ERP from an electrode placed over the somatosensory cortex (location shown in the inset) is shown in black while individual ERPs are shown in grey. The analytical baseline period is shaded in grey. Right: black line indicates the grand-averaged global field power (GFP) while grey lines indicate individual's GFP. The period of the signal used in the subsequent analysis is shaded in yellow (Time period of interest, TOI). (C) Population-wide averaged EEG independent components based on k-means clusters that use the putative dipole locations (n = 433). We identified 12 clusters, each representing a putatively distinct brain process – the cluster order is preserved throughout the manuscript for cross-referencing.

Cortical signals cluster according to the next-interval smartphone interaction statistics

We captured the next-interval statistics of smartphone interactions recorded during the measurement section using the JID framework (Fig 2A). Here, the previous interval (say *k*) is represented along with the penultimate interval (say *k*-1). There was substantial variation in these distributions from one person to the next (see Fig 2B). The population average distribution was dominated by consistent next-interval durations of ~ 1 s. This pattern is in keeping with what is generally observed outside of the laboratory (33).

At the individual level, source-separated cortical signals were time-locked to smartphone interactions (SI), yielding a trial-by-trial ERP matrix for each independent component (IC-ERP). These matrices exhibited substantial trial-to-trial variation. To identify underlying prototypical patterns from a high-dimensional neural matrix, we applied non-negative matrix factorization (NNMF), obtaining a parts-based lower-dimensional representation (Fig. 2C). This pipeline progresses from raw EEG signals to source-separated components, then to prototypical neural response patterns, and finally to behavioral clustering within JID space. This analysis decomposed IC-ERPs into a set of prototypical time-varying neural patterns (meta-IC-ERP) and corresponding weights for each trial (meta-SI). For each of these prototypical patterns, we then segregated the meta-SI weights according to each trial's position in the JID, defined by the previous interval ending at that interaction (*k*) and the penultimate interval (*k*-1). This revealed 'neuro-behavioral clusters' of next-interval statistics (meta-JISI) for each meta-IC-ERP—that is, touchscreen interactions with similar next-interval dynamics shared similar meta-SI weights i.e., common neural signal features. In simple terms, this analysis asked: do interactions with similar interval dynamics recruit similar neural patterns? For instance, in Participant 11, an independent component (Fig. 2D) exhibited a neural pattern peaking ~1 s pre-touch that clustered with intervals <1 s, and a second pattern peaking at +85 ms that clustered with intervals >1 s. Moran's I confirmed the significant neuro-behavioral clustering (positive values indicate similar values cluster together) relative to bootstrapped null distributions (Fig. 2D). This means that specific neural patterns were systematically aligned to particular behavioral patterns rather than randomly distributed across all behavioral responses.

Across the population, we identified a variety of neuro-behavioral clusters in the meta-JISI space (Fig. 2E and F). The exact nature of clusters varied across participants and independent components. Most participants (50 out of 53) showed at least one significant neuro-behavioral cluster, with a median of 3 significant clusters per person. We grouped independent components according to their dipole locations to examine the regional distribution in neuro-behavioral clustering (Fig. 2F). Regions most frequently showing neuro-behavioral clusters were occipital regions (Group 1, 65.71% of participants), cingulate cortex (Group 2, 57.45%),

sensorimotor regions (Group 3, 58.06%), and parietal cortex (Group 9, 66.67%). Having established that next-interval statistics organize neural activity across multiple brain regions, we next examined the transient nature of the neuro-behavioral clusters.

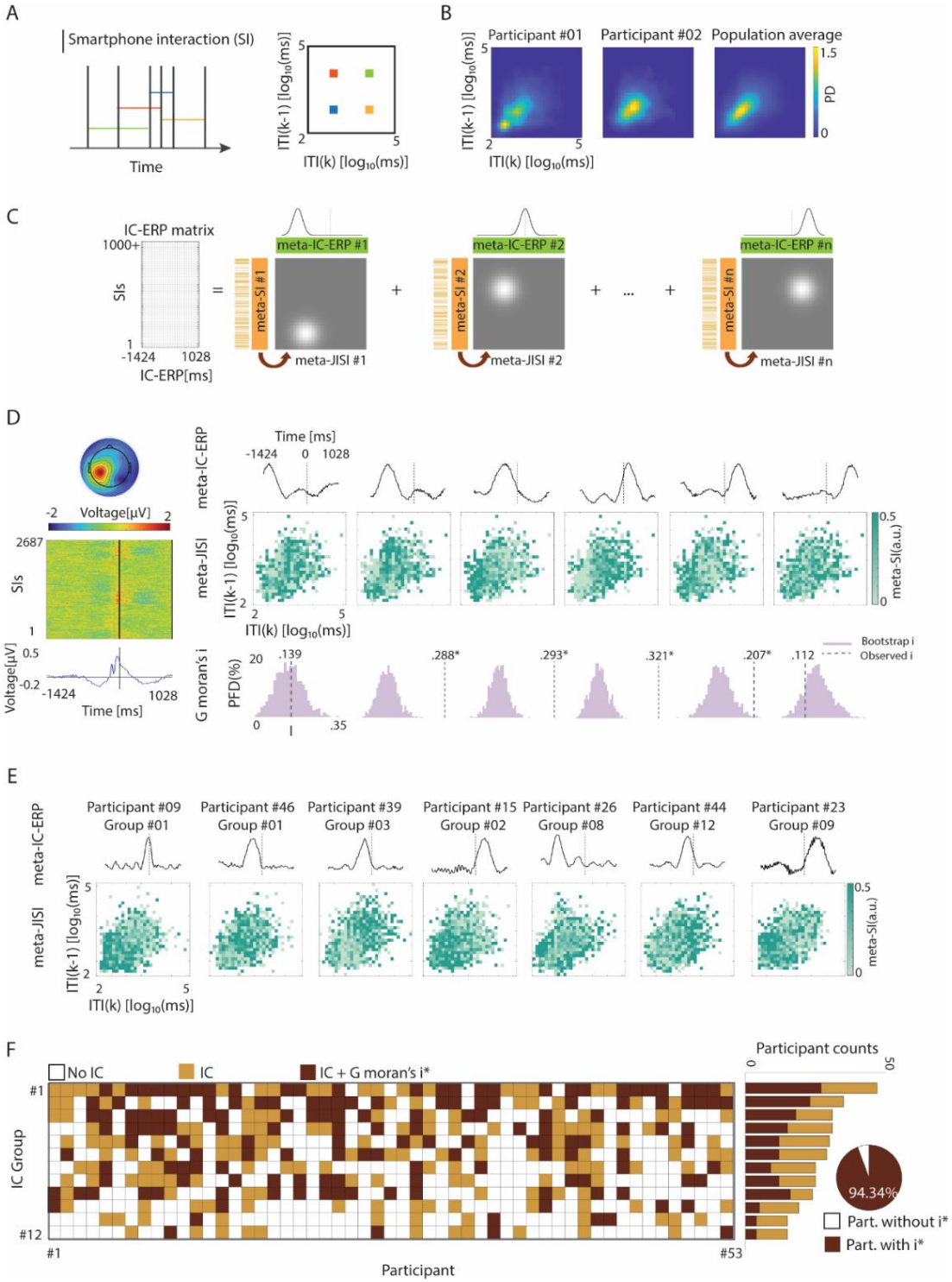

Figure 2. Neuro-behavioral clusters of cortical signals aligned to smartphone next-interval statistics. (A) A schematic explanation of how next-interval statistics of smartphone interactions are captured using a behavioral map: the joint-interval distribution (JID) approach. (B) The next-interval statistics of smartphone interactions were captured

during the EEG measurement session. To illustrate the inter-individual differences, the JID from two participants (Sub#01 and #02) are shown, and averaged JID stemming from the sampled population (n = 53). (C) Schematic explanation of parts-based reduction of the neural signals time-locked to smartphone interactions. The source-separated cortical signals were time-locked to the smartphone interactions (SIs) resulting in a signal matrix of interactions number x EEG signal latency. We extracted a lower-rank approximation of the matrix using non-negative matrix factorization (NNMF). The reduced prototypical patterns were meta-IC-ERPs – the time-varying neural signal feature – and the corresponding value indicating to what extent the neural feature was present for a given smartphone interaction (meta-SI). The meta-SI values were then separated according the next-interval statistics of the JID yielding a meta–joint-interval smartphone interaction (meta-JISI). (D) Example of neuro-behavioral clusters derived from IC Group #6 of participant #11. Left panel: IC topography, interaction-by-interaction IC-ERPs and the average IC-ERP across interactions. Right panel: six neuro-behavioral clusters identified for this IC. Top and middle: Meta-IC-ERPs and the corresponding meta-JISIs. Bottom: The meta-JISIs were then tested for 2D temporal autocorrelation using Moran's I: an index of how similar the temporal neighborhood is in terms of the meta-JISI values. This value (dashed line) was contrasted to the null distribution of bootstrap shuffled I values – revealing 4 out of 6 meta-JISIs clustered distinctly from the chance levels. This demonstrates that specific neural patterns were aligned with particular behavioral patterns rather than randomly distributed across all behavioral responses. (E) Across the population we found a range of neuro-behavioral clusters. These example clusters stem from different participants and source-separated cortical processes. (F) Overview of the source-separated cortical processes which were found to be clustered in the meta-JISI, i.e., a neural process aligned to the next-interval statistics. Each row depicts a participant and the column depicts the source-separated cortical process. The brown-filled grid indicates a source-separated cortical signal that showed significant 2D temporal autocorrelation and the yellow grid indicates an absence of the same. A white grid indicates the absence of a source-separated process for the corresponding IC group. Bar plots indicate the participant counts with and without significant autocorrelations. The pie chart indicates the prevalence of significant 2D temporal autocorrelation in the sampled population.

Time course of the emergent neuro-behavioral clusters

Our dimensionality reduction approach identified the behavioral specificity of clusters (meta-JISI) and their temporal evolution (meta-IC-ERP). The timing of each meta-IC-ERP peak reveals when that cluster's neural pattern is most prominent. Analyzing peak latencies across all meta-IC-ERPs and participants revealed the temporal organization of interval-specific neural processing.

First, we addressed whether the clusters were more likely to occur before or after the touchscreen interaction. At the level of the population and pooling across all the brain signal sources (ICs from Group#1-12), we calculated the clustering rate for each individual (peak counts/observation duration) and found that the clustering rate was 0.0037 (SD=0.0030) prior to the smartphone interaction and 0.0016 (SD=0.0017) after the interaction (Fig. 3A). A paired t-test revealed that the clustering rate was significantly higher prior to the interaction than after ($t(52) = 6.1690$, $p = 1.04\times10^{-7}$, 95% CI [0.0014 0.0027]). This pattern of increased rate of neuro-behavioral clustering prior to the interaction was also evident when pooling all the meta-IC-ERPs stemming from all IC groups (Group#1-12, Fig. 3B), as the observed proportion of pre-interaction peaks ($\hat{p}$=0.76) exceeded the expected pre-interaction probability (p_0=0.58) under a uniform temporal null model, as confirmed by a one-sided binomial test (p<.05). Next, to address whether this pattern was constrained to a specific source-separated cortical signal, we separately examined the meta-IC-ERPs stemming from each IC group. Here the peak-time distributions indicated a pre-interaction prominence for the first three IC clusters using one-sided binominal tests comparing observed and expected pre-interaction probabilities:

spanning the occipital regions, the cingulate cortex regions and the sensorimotor regions (p<.05). In sum, the neuro-behavioral clustering is more common before the smartphone interaction than after - and this property extends to multiple source-separated neural signals (ICs). These findings underscore the anticipatory nature of cortical responses to smartphone interactions, reflecting the brain's readiness and heightened activity before engaging in touchscreen behavior. Next, and finally, we will address which behaviors were more likely to participate in the neuro-behavioral clusters discovered here.

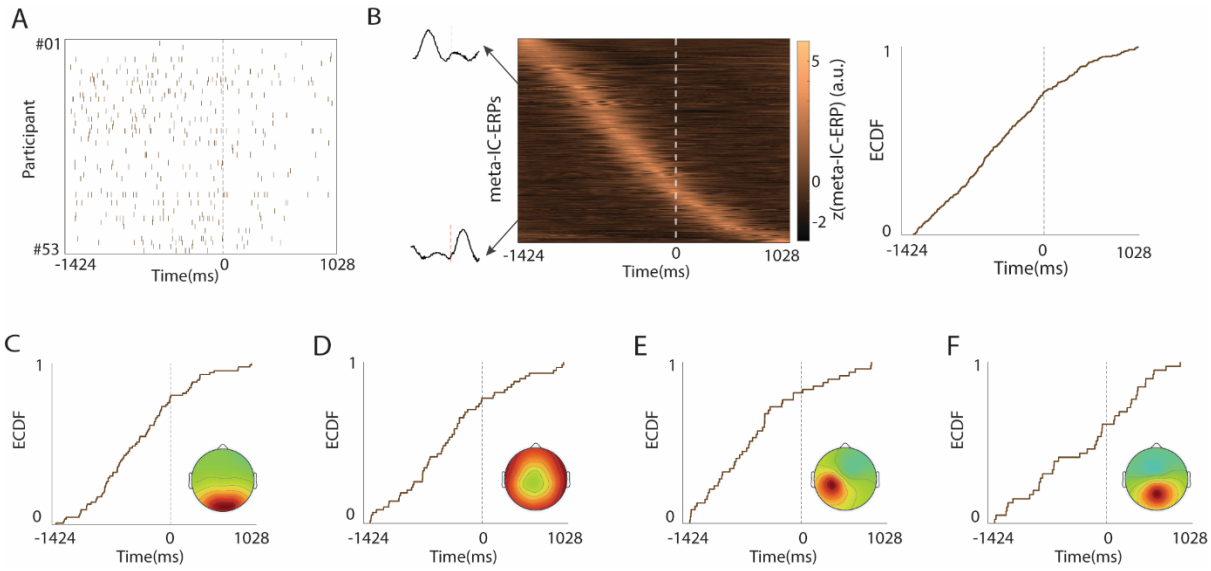

Figure 3. Latency of neuro-behavioral clusters relative to smartphone interaction. (A) The distribution of meta-IC-ERP peak latencies corresponding to all the neuro-behavioral clusters observed in each participant (rows). The distribution is time-locked to the smartphone interaction (dashed line). (B) Left: meta-IC-ERPs pooled from all the participants across all neural processes clusters. The data is sorted according to the peak times. Right: The empirical cumulative distribution function (ECDF) of the peak times. (C-F) The peak times based on meta-IC-ERPs pooled from all the participants and the four most prevalent clusters (#1, #2, #3, #9; the inserts show scalp locations per cluster).

Heterogeneous representation of behaviour in neuro-behavioral clusters

By tracking the location of neuro-behavioral clusters in the behavioral map (meta-JISI), we identified which specific interval dynamics participated in clustering. We applied local Moran's I to identify locations within each meta-JISI exhibiting moderate or high spatial autocorrelation with their neighbors (I $\geqslant$ 0.3) and enclosed these locations in contours demarcating cluster boundaries. In total, we identified 366 contours from 53 participants across all independent components.

First, for each bin in the behavioral map, we estimated the probability of cluster participation (I $\geqslant$ 0.3) across all meta-JISIs pooled across participants (Fig. 4A). This revealed reduced clustering probability for intermediate consecutive intervals, forming an annular pattern in the

descriptive behavioral map. Notably, this pattern persisted when separating neural processes occurring before versus after the interaction (Fig. 4B and C). Second, we characterized the temporal span of clusters—the range of timescales occupied by each cluster. Focusing on the largest neuro-behavioral clusters (>4 bins) delineated by local Moran's I in each meta-JISI, we found substantial variation: some clusters comprised behaviors with intervals of a few hundred milliseconds, while others spanned timescales from milliseconds to several seconds (Fig. 4D). The span appeared similarly broad whether the processes were before or after the interaction (Fig. 4E and F).

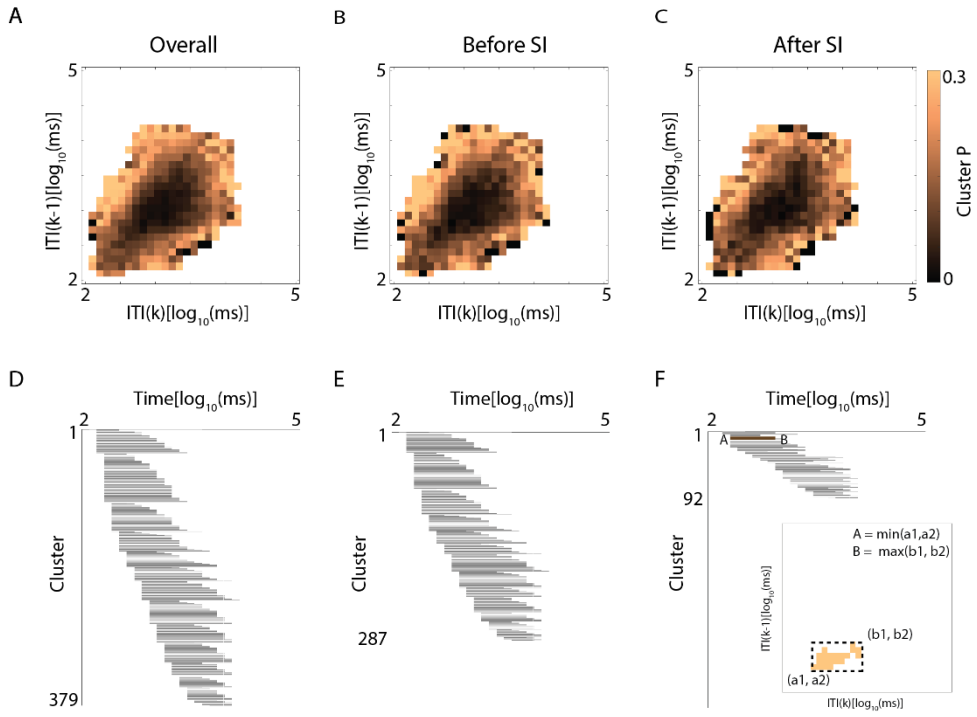

Figure 4. Description of the behaviors engaged in the neuro-behavioral clusters. (A) Probability of a given two-dimensional bin participating in a neuro-behavioral cluster pooled across all ICs and participants. In this pooled set, we estimated the probability of any two-dimensional bin contributing to a cluster according to local Moran's I (I ⩾ 0.3). (B-C) Same as (A) except that here we pooled only those clusters which formed before (B) or after (C) smartphone interaction (SI). (D) Time-scale spans of all clusters across all binary meta-JISIs. Each grey line represents the time-scale span of a single cluster on the behavioral map. Clusters were included if they contained more than four two-dimensional bins. (E–F) Same as (D), but clusters were grouped based on whether the corresponding meta-IC-ERP peaks occurred before (E) or after (F) SI. Insert in F illustrates the definition of the cluster span used in D-F.

Discussion

Smartphone touchscreen interactions produce rich temporal patterns spanning hundreds of milliseconds to several seconds. We found that neural activity surrounding touchscreen interactions is organized into behavioral maps clustering interval statistics—a principle that held across participants spanning the adult lifespan. Notably, while similar interval dynamics (on a logarithmic scale) clustered together, individual clusters often spanned multiple temporal

scales, suggesting neural processes that integrate timing information across scales from milliseconds to seconds. These maps varied across processing stages and brain regions (frontal to occipital cortex) and were temporally dynamic—emerging predominantly before touches, and becoming sparser afterward. Our findings reveal how the brain organizes diverse behavioral outputs: interval-based maps create transient low-dimensional representations that span temporal scales to facilitate action planning and execution.

These smartphone behavioral maps offer a key extension to the idea that interval patterns provide an organizing principle. In designed laboratory tasks with speeded responses, there is a rough separation in neural processing of sub-second versus supra-second intervals (29). Our data provides a more fine-grained account where behaviors are clustered according to their next-interval statistics. Furthermore, some clusters spanned multiple timescales, challenging a simple separation between slow versus fast behaviors and suggesting common neural processes that integrate across temporal scales.

The neuro-behavioral clusters were transient, lasting less than a second. This suggests that low-dimensional behavioral maps serve different functions across processing stages surrounding touchscreen interaction. The touchscreen event provided a temporal landmark to examine whether pre-interaction and post-interaction cluster dynamics differed systematically. Prior event-related potential observations indicate that pre-interaction stages are dominated by preparatory sensorimotor processes whereas post-interaction stages involve information processing and consolidation (32). Because neuro-behavioral clusters were more prevalent before interactions than after, we speculate that the preparatory stages of information processing leverage the recent temporal statistics to guide the ongoing behavior.

Our results support the idea that temporal structure is encoded by distributed cortical regions (21, 23, 29). Neuro-behavioral clusters were evident across multiple brain areas, from frontal cortex supporting motor planning to occipital cortex processing visual information. This cortex-wide tuning to next-interval statistics does not rule out the presence of specialized neural circuits for tracking time. For instance, the secondary somatosensory cortex has been previously implicated in tracking tactile temporal patterns, and it may distribute this information to the rest of the cortex (34). However, if such a distribution alone was in use, then the same behavioral clusters would reoccur across the source-separated signals (ICs) - which was not observed.

Our findings suggest why behavioral clusters in prior JID studies correlate with age and disease: these clusters may reflect shared neural processes. When aging or pathology affects a neural process, it would impact all behaviors within its associated cluster. Remarkably, the brain may employ the same low-dimensional interval mapping we used for analysis. While we

do not claim that the brain explicitly constructs a JID-like map, our findings indicate that neural dynamics are systematically organized according to the same interval statistics captured by this framework. Just as the JID provides an analytical framework to organize complex temporal patterns, the brain may use similar interval-based maps to parse ongoing behavior and efficiently allocate neural resources to behaviors with similar timing statistics. However, the most common consecutive intervals rarely formed neuro-behavioral clusters, creating a ring-like gap in the pooled cluster distribution. This suggests clustering may be less important for routine temporal patterns and more critical for organizing less frequent or more complex behavioral sequences. Alternatively, the brain may employ a representational strategy based on higher-dimensional temporal patterns to organize more frequent behaviors, which may not to be adequately captured by this 2D JID space.

How do neuro-behavioral clusters form? Use-dependent plasticity provides a candidate mechanism: temporal statistics might shape neural organization through experience. Critically, however, the relationship is non-linear—the most frequently occurring intervals showed minimal clustering. This paradox suggests that clusters may reflect learning of behaviorally relevant patterns rather than passive accumulation of frequent experiences. Such use-dependent formation would naturally produce the substantial inter-individual differences we observed, as each person's smartphone usage creates unique temporal statistics. This interpretation is consistent with use-dependent cortical plasticity from smartphone use (35, 36), underscores the necessity of individual-level analysis for real-world neuroscience (37, 38), and contributes to growing evidence for marked individual differences in brain-behavior relationships (39–43).

Understanding how the brain generates behavior is fundamental to neuroscience, yet the field has relied predominantly on artificial laboratory tasks with speeded responses. Smartphone interactions provide a powerful alternative: discrete, measurable actions (taps, swipes) that serve complex functions and exhibit rich temporal structure across multiple timescales –dynamics absent from conventional laboratory paradigms. This narrow temporal window in traditional tasks may explain why interval-based behavioral maps have remained undiscovered, although prior work using restricted ranges has hinted at a coarse separation between slow versus fast behaviors (24). We reveal that when natural temporal dynamics are preserved, the brain creates transient low-dimensional maps organizing behavior by interval statistics across timescales – temporal analogs to established sensory maps like tonotopy or retinotopy. These maps integrate recent behavioral history to guide ongoing action. Future research must determine how temporal maps interact with other neural representations, how they emerge through experience, how they alter across the lifespan, and how they enable real-world computation. The smartphone provides an unprecedented

window into these questions, capturing the neural basis of human behavior as it naturally unfolds.

Method

Participants

Sixty-four participants (age range: 20-81 years; 40 females) were recruited from a participant pool via agestudy.nl research platform (33). All participants had no neurological or psychiatric health disorders according to a self-reported screening at enrolment. Four participants were excluded due to a change in self-reported health status: they had developed tinnitus, stroke, arthrosis, or psychiatric disorder. All participants provided written informed consent. This study was approved by the Ethics Committee of Psychology at Leiden University (ERB-reference number: 2020-02-14-Ghosh, dr. A.-V2-2044).

Smartphone data collection

Smartphone behavior was recorded via the TapCounter app (QuantActions AG, Switzerland) (44). All participants accumulated at least one month of smartphone data before EEG measurement. The app logged each interaction timestamp in UTC milliseconds in the background. During EEG recordings, participants freely used one of their four most-used apps from the past month, and switched apps every 10 min after a short break. They were asked to use only their right thumb to touch the screen during measurement. Two experimenters monitored participants using a camera and offered the reminder to use the right thumb when participants deviated. The interactions were stored on a cloud-based data management platform after the EEG measurement. Two participants were excluded because of missing smartphone data on this platform for unknown reasons.

Movement recording and time alignment

Thumb kinematics was captured using a movement sensor while on the smartphone (Flex Sensor, 112 mm, Digi-Key, Thief River Falls, USA). The sensor was attached to participants' right thumb's dorsum using a custom-made jacket. Using this configuration participants were able to freely move their right thumb to interact with smartphone. Analog signals from the movement sensor were sampled at 1 kHz by using a Polybox (Brain Products GmbH, Gilching, Germany) that fed into a digitizer running on the same clock as used for the EEG signals (see below). The continuous movement signal was band-pass filtered between 1 and 10 Hz and then epoched using a 6 s window centered surrounding each interaction and averaged movement signals across trials for each participant.

The smartphone operating system and EEG acquisition system operated on independent clocks requiring post-hoc alignment. We synchronized these clocks using movement kinematics as a bridge signal as described before (1). Briefly, movement kinematics (thumb movements) were recorded concurrently with EEG. A pre-trained kinematic-to-touch model predicted touchscreen event times from movement data, successfully identifying the majority of actual events. We then aligned the smartphone and EEG time bases by matching predicted event times (in EEG time) to logged event times (in smartphone time). Four participants were excluded due to poor model performance as confirmed by the average movement sensor signal trace. For participants with multiple recording sessions, the predicted interaction time may differ between the sessions due to subtle kinematic differences impacting the movement profile. We utilized the *alignsignals* function with the *xcorr* method to align the movement waveforms to the waveform whose negative peak occurred closest to the touch time (Matlab's Signal processing toolbox, MathWorks, Natick, MA, USA). We then calculated the correlation between these time-corrected datasets using Pearson's correlation coefficient – where high correlation indicates successful alignment across sessions. Datasets with a correlation value below 0.71 were excluded from further analysis. This threshold was determined using the elbow method (45) applied to the empirical cumulative distribution (ECDF) of correlation values across participants. This ECDF line showed a clear 'elbow' point at $r = 0.71$, indicating a transition from highly variable to more stable and consistent correlations. Therefore, only datasets with $r \geqslant 0.71$ were retained in further analysis.

EEG recording and preprocessing

EEG data were collected using a 64-channels active cap (62 scalp electrodes, 2 ocular electrodes) with a customized equidistant layout (ActiCap Snap, EasyCap Gmbh, Wörthsee, Germany). The EEG signals from the active cap system were referenced to the vertex and amplified with a BrainAmp amplifier (Brain Products GmbH, Gilching, Germany), and digitized at a 1 kHz sampling rate. Participants arrived with clean, washed hair and scalp. The scalp contact sites were further degreased using alcohol swabs. Supervisc gel (Easycap GmbH, Herrsching, Germany) was applied to electrically bridge the skin to the electrode, with electrode impedance targeted below 10 kΩ. The data was processed using the EEGLAB toolbox (46), signal processing toolbox (MATLAB, Mathworks, Natick) and custom scripts in MATLAB 2023b (MATLAB, Mathworks, Natick). The raw data was high-pass filtered at 0.5 Hz. Inactive smartphone use data segments (pre-interval & post-interval >60 s, for instance resulting from checking in with the participant or offering a drink break) were removed from the analysis.

At the individual level ERPs were computed after low-pass filtering at 20 Hz and removing of the artefacts based on ICA results when over 80% likelihood originating from artifacts like blinks, muscles, etc., as evaluated by ICLabel toolbox (47). Cleaned EEG data were then epoched from -3 to 3 s relative to smartphone interaction time. Baseline correction was performed by subtracting the signal mean from -3 to -1.5 s. Grand-averaged ERP signals were then calculated.

To identify the time period of interest (TOI) of event-evoked potentials, we utilized the global field power (GFP), which is a time-variant reference independent indicator of activity based on all of the electrodes (48). Here, for each individual, we calculated the averaged ERP for each electrode across trials after trimming extreme value with trimean function. Next, we calculated the standard deviation of ERP across channels at each timepoint (from -3s to 3s with 1ms step). Then, we obtained the grand-averaged GFP (z-transformed) by averaging across participants. To identify the change points of the grand-averaged GFP wave, we utilized the *findchangepts* function with the standard division statistic method and a maximum of two change points (Matlab's Signal processing toolbox, MathWorks, Natick). The period between these two change points, -1424 and 1048 ms, were defined as the TOI. The IC-ERPs matrix (see below) was limited to this window for subsequent analysis.

Identifying brain signal sources

We decomposed diverse brain signal sources from the continuous and pre-processed EEG data by adaptive mixture independent component analysis (AMICA) with 2,000 maximum iterations (49, 50). We estimated the equivalent current dipoles and residual variance for each independent component (IC) using the *DIPFIT* toolbox (51). ICs with dipole locations outside of the brain or if the dipole model explained less than 85% of the IC's scalp voltage distribution (residual variance >15%) were excluded. We further excluded ICs with less than 50% likelihood originating from brain source, as evaluated by the *ICLabel* toolbox (47). One participant was excluded due to no surviving IC after screening. Then, the remaining ICs (n=433) from 53 participants were clustered using the *Kmeans* method based on equivalent dipole locations. We explored cluster ranks from 3 to 40, and evaluated the optimal cluster rank using the *evalclusters* function with the 'Silhouette' method implemented in MATLAB (Statistics and Machine Learning Toolbox, MathWorks, Natick). Given the variability introduced by random initialization, we repeated this evaluation procedure 100 times and identified the most frequently selected cluster rank as the final optimal cluster rank. To get a reproducible reduction output using the optimal rank approach, we conducted 1,000 repetitions, each with maximum 10,000 iterations. The final reduction results were selected from the repetition with the best sum of squared distance. Source-separated independent

496 component ERP (IC-ERP) matrix was then reconstructed using *eeg_getdatact (*EEGLAB
497 toolbox*,* Delorme and Makeig, 2004*)* based on the cleaned epoched EEG data with the
498 window of TOI, resulting in a rich neural signals matrix of C (components) × T (latencies) × I
499 (smartphone interactions) for each participant.

500 *Smartphone joint-interval distribution (JID)*

501 Interval durations between smartphone interactions were then calculated, ranging from
502 hundreds of milliseconds to a few seconds. The rich and continuous smartphone behavior can
503 be separated according to the next-interval dynamics using the joint-interval distribution (JID)
504 approach (see Fig. 2A), yielding a behavioral map (11). In brief, we established a two-
505 dimensional space where the x-axis represents the pre-interval (say K) while the y-axis
506 represents the penultimate interval (say K-1) in a logarithmic scale spanning from 100 ms to
507 10 s. We further binned the space into 30 units along the x-axis and y-axis, respectively,
508 resulting in 900 two-dimensional pixels.

509 *Identifying neuro-behavioral clusters*

510 For any source-separated cortical signal (for instance, Fig. 2C), there was substantial variation
511 from one smartphone interaction to the next, and this was captured in a neural signal matrix
512 organized as the number of interactions x TOI. We extracted the patterns distributed in this
513 rich matrix by using data-driven dimensionality reduction – by using a variant of non-negative
514 matrix factorization (NNMF, (52)). The stable and reproducible NNMF (starNNMF) was used
515 to yield time-varying neural features (*meta-IC-ERP*) that occur at different levels across
516 smartphone interactions (*meta-SI*). This method is detailed elsewhere (53). In brief, we
517 obtained a non-negative IC-ERP matrix by subtracting the minimum IC-ERP value from the
518 whole matrix. Next, for each participant and source-separated cortical process, we applied the
519 NNMF to the matrix and then searched for the optimal cluster ranks (*c*) between 2 to 15
520 clusters with 100 repetitions. We identified the optimal *c* which has the minimum error between
521 the real matrix and the reconstructed matrix. Then, with optimal *c* identified, we obtained stable
522 and reproducible decomposition based on 1000 repetitions. Next, the meta-SI was analyzed
523 in the context of next-interval statistics to reveal how distinct neural processes, activated at
524 specific latencies, map onto the smartphone temporal patterns captured using the JID. For
525 each pixel, we calculated the median value of meta-SIs, thus yielding a meta-JISI
526 representation.

527 To assess whether the distribution of behavioral map (meta-JISI) was randomly patterned or
528 showed two-dimensional autocorrelations, we adopted the global Moran's I (54). This
529 autocorrelation method is typically utilized to identify spatial autocorrelations but the

underlying math can be applied to any two-dimensional representation and capture the similarity with its neighborhood (54). In brief, we calculated the global Moran's I for the meta-JISI and a null distribution of I's based on shuffled ordered trials (1000 permutations). A one-sample t-test (α=0.05) was conducted to compare the real vs. the bootstrapped I's. The neuro-behavioral clusters with a value of I distinct from the null distribution was extracted for further analysis. In a related analysis, we localized the two-dimensional bins participating in the autocorrelations by using local Moran's I (55).

To address the timing of the neuro-behavioral clusters, we focused on the distribution of meta-IC-ERP peak latencies. We calculated the clustering rate before ($\frac{no.\ of\ peaks}{pre-interaction\ TOI}$) and after ($\frac{no.\ of\ peaks}{post-interaction\ TOI}$) the touchscreen interaction for each individual and contrasted it by using a paired t-test. A separate method was also used to address the same. Towards this, we pooled meta-IC-ERPs across participants and estimated the empirical cumulative distribution function (ECDF) of the peak latencies. Here, pre vs. post touch rate differences were assessed using one-sided binomial test (α =0.05) to compare the observed proportion of pre-touch peaks ($\hat{p}$=$\frac{no.\ of\ peaks\ during\ pre-interaction}{no.\ of\ peaks}$) with expected pre-touch probability under a uniform temporal null model (p_0=$\frac{pre-interaction\ TOI}{TOI}$). This approach was also used at the level of each IC group i.e., where the meta-IC-ERPs were selectively pooled across the IC groups.

We established clusters in the meta-JISI using Moran's I – which is well established for quantifying spatial auto-correlations such as in geographical data. The real I for each meta-JISI was tested against a corresponding bootstrapped null distribution based on shuffled data (1000 bootstraps). To localize the clusters we used a related approach (local Moran's I) that revealed two-dimensional bins which contribute to moderate or high autocorrelations (local moran's I >0.3). We then binarized the local Moran's I matrix by assigning 1 to local Moran's I ≥ 0.3 and 0 otherwise. We then averaged these binary values for each two-dimensional bin of the JID. The same analysis was performed separately for meta-JISI that occurred before and after smartphone interaction. Finally, we quantified the time-scale occupied by the clusters. By using *bwconncomp* in MATLAB, we identified clusters from all binary meta-JISI and focused on the largest cluster (> 4 bins). This threshold was determined by using the elbow method based on the distribution of pooled cluster sizes. For each cluster, we estimated the time-scale span by extracting the minimum and maximum coordinates of its constituent bins. The same analysis was also performed separately for the clusters before and after smartphone interaction.

Data, Materials, and Software Availability

The data will be available on dataverse.nl upon publication. The custom-written scripts used towards this report are shared on: https://github.com/CODELABCODELIB/JID_ERP_Smartphone_2024.

Acknowledgements

This project was funded by Velux Stiftung (Grant No.1283, awarded to A.G. with Richard Ridderinkhof as co-applicant). We acknowledge Beste Yavuz, Lysanne Groenewegen, Barbora Michalidesová, Lorenzo Van Hoorde for their help with EEG data collection. We also thank all participants for contributing their time and effort. The authors used Claude (Anth ropic, Claude Sonnet 4.5, accessed January 2026) to improve the clarity, grammar, and organization of the manuscript text. The AI was used solely for language editing; all scientific content, study design, data collection and analysis, interpretation of results, and conclusions were developed by the authors who take full responsibility for the accuracy and integrity of the manuscript.

Author contributions

A.G. conceived the study. A.G. and W.W. designed the study. W.W acquired, performed EEG pre-processing and analyzed the data with the aid of A.G.. W.W drafted with the aid of A.G. K.R.R., A.G., W.W. edited the manuscript.

Declaration of interests

A.G. is a co-founder and chairman of QuantActions AG, and is an advisor for Axite B.V. W.W., K.R.R. declare no competing interests.

Reference

1. R. Kock, E. Ceolini, L. Groenewegen, A. Ghosh, Neural processing of goal and non-goal-directed movements on the smartphone. *Neuroimage: Reports* **3**, 100164 (2023).

2. J.-P. Pfister, A. Ghosh, Generalized priority-based model for smartphone screen touches. *Phys. Rev. E* **102**, 012307 (2020).

3. A. Vázquez, *et al.*, Modeling bursts and heavy tails in human dynamics. *Phys. Rev. E* **73**, 036127 (2006).

4. E. Ceolini, K. R. Ridderinkhof, A. Ghosh, Age-related behavioral resilience in smartphone touchscreen interaction dynamics. *Proceedings of the National Academy of Sciences* **121**, e2311865121 (2024).

5. E. Ceolini, R. Kock, G. P. H. Band, G. Stoet, A. Ghosh, Temporal clusters of age-related behavioral alterations captured in smartphone touchscreen interactions. *iScience* **25**, 104791 (2022).

6. E. Ceolini, *et al.*, A model of healthy aging based on smartphone interactions reveals advanced behavioral age in neurological disease. *iScience* **25**, 104792 (2022).

7. A. R. van Nieuw Amerongen, A. M. Meppelink, A. Ghosh, R. D. Thijs, Real-world smartphone data can trace the behavioural impact of epilepsy: A case study. *European Journal of Neurology* **31**, e16433 (2024).

8. M. Fishman, *et al.*, A method for analyzing temporal patterns of variability of a time series from Poincaré plots. *Journal of Applied Physiology* **113**, 297–306 (2012).

9. P. Holmes, Poincaré, celestial mechanics, dynamical-systems theory and "chaos." *Physics Reports* **193**, 137–163 (1990).

10. R. W. Rodieck, N. Y.-S. Kiang, G. L. Gerstein, Some Quantitative Methods for the Study of Spontaneous Activity of Single Neurons. *Biophysical Journal* **2**, 351–368 (1962).

11. R. B. Duckrow, E. Ceolini, H. P. Zaveri, C. Brooks, A. Ghosh, Artificial neural network trained on smartphone behavior can trace epileptiform activity in epilepsy. *iScience* **24** (2021).

12. E. Ceolini, A. Ghosh, Common multi-day rhythms in smartphone behavior. [Preprint] (2022). Available at: https://www.biorxiv.org/content/10.1101/2022.08.25.505261v1 [Accessed 2 October 2022].

13. J. R. Saffran, R. N. Aslin, E. L. Newport, Statistical Learning by 8-Month-Old Infants. *Science* **274**, 1926–1928 (1996).

14. N. B. Turk-Browne, "Statistical Learning and Its Consequences" in *The Influence of Attention, Learning, and Motivation on Visual Search*, M. D. Dodd, J. H. Flowers, Eds. (Springer, 2012), pp. 117–146.

15. K. Friston, A theory of cortical responses. *Philos Trans R Soc Lond B Biol Sci* **360**, 815–836 (2005).

16. R. P. N. Rao, D. H. Ballard, Predictive coding in the visual cortex: a functional interpretation of some extra-classical receptive-field effects. *Nat Neurosci* **2**, 79–87 (1999).

17. C. Summerfield, F. P. de Lange, Expectation in perceptual decision making: neural and computational mechanisms. *Nat Rev Neurosci* **15**, 745–756 (2014).

18. K. J. Friston, T. Parr, B. de Vries, The graphical brain: Belief propagation and active inference. *Network Neuroscience* **1**, 381–414 (2017).

19. K. R. Ridderinkhof, Neurocognitive mechanisms of perception–action coordination: A review and theoretical integration. *Neuroscience & Biobehavioral Reviews* **46**, 3–29 (2014).

20. D. Bueti, S. Lasaponara, M. Cercignani, E. Macaluso, Learning about time: plastic changes and interindividual brain differences. *Neuron* **75**, 725–737 (2012).

21. D. V. Buonomano, R. Laje, Population clocks: motor timing with neural dynamics. *Trends in cognitive sciences* **14**, 520–527 (2010).

22. A. Goel, D. V. Buonomano, Timing as an intrinsic property of neural networks: evidence from in vivo and in vitro experiments. *Philosophical transactions of the Royal Society B: Biological sciences* **369**, 20120460 (2014).

23. U. R. Karmarkar, D. V. Buonomano, Timing in the absence of clocks: encoding time in neural network states. *Neuron* **53**, 427–38 (2007).

24. J. J. Paton, D. V. Buonomano, The Neural Basis of Timing: Distributed Mechanisms for Diverse Functions. *Neuron* **98**, 687–705 (2018).

25. A. Hernández, *et al.*, Decoding a perceptual decision process across cortex. *Neuron* **66**, 300–314 (2010).

26. C. K. Machens, R. Romo, C. D. Brody, Flexible control of mutual inhibition: a neural model of two-interval discrimination. *Science* **307**, 1121–1124 (2005).

27. G. Koch, M. Oliveri, C. Caltagirone, Neural networks engaged in milliseconds and seconds time processing: evidence from transcranial magnetic stimulation and patients with cortical or subcortical dysfunction. *Philos Trans R Soc Lond B Biol Sci* **364**, 1907–18 (2009).

28. P. A. Lewis, R. C. Miall, Brain activation patterns during measurement of sub- and supra-second intervals. *Neuropsychologia* **41**, 1583–92 (2003).

29. J. J. Paton, D. V. Buonomano, The Neural Basis of Timing: Distributed Mechanisms for Diverse Functions. *Neuron* **98**, 687–705 (2018).

30. E. A. Petter, N. A. Lusk, G. Hesslow, W. H. Meck, Interactive roles of the cerebellum and striatum in sub-second and supra-second timing: Support for an initiation, continuation, adjustment, and termination (ICAT) model of temporal processing. *Neuroscience & Biobehavioral Reviews* **71**, 739–755 (2016).

31. W. Wan, K. R. Ridderinkhof, A. Ghosh, The timing of preceding tactile inputs modulates cortical processing. *Imaging Neuroscience* in press (2026).

32. R. Kock, E. Ceolini, L. Groenewegen, A. Ghosh, Neural processing of goal and non-goal-directed movements on the smartphone. *Neuroimage: Reports* **3**, 100164 (2023).

33. E. Ceolini, R. Kock, G. P. H. Band, G. Stoet, A. Ghosh, Temporal clusters of age-related behavioral alterations captured in smartphone touchscreen interactions. *iScience* **25** (2022).

34. R. Rossi-Pool, A. Zainos, M. Alvarez, G. Diaz-deLeon, R. Romo, A continuum of invariant sensory and behavioral-context perceptual coding in secondary somatosensory cortex. *Nature communications* **12**, 2000 (2021).

35. M. Balerna, A. Ghosh, The details of past actions on a smartphone touchscreen are reflected by intrinsic sensorimotor dynamics. *npj Digital Med* **1**, 1–5 (2018).

36. A.-D. Gindrat, M. Chytiris, M. Balerna, E. M. Rouiller, A. Ghosh, Use-Dependent Cortical Processing from Fingertips in Touchscreen Phone Users. *Current Biology* **25**, 109–116 (2015).

37. K. Akiti, *et al.*, Striatal dopamine explains novelty-induced behavioral dynamics and individual variability in threat prediction. *Neuron* **110**, 3789-3804. e9 (2022).

38. D. R. Levy, *et al.*, Mouse spontaneous behavior reflects individual variation rather than estrous state. *Current Biology* **33**, 1358-1364. e4 (2023).

39. E. S. Finn, *et al.*, Functional connectome fingerprinting: identifying individuals using patterns of brain connectivity. *Nature neuroscience* **18**, 1664–1671 (2015).

40. R. Kanai, G. Rees, The structural basis of inter-individual differences in human behaviour and cognition. *Nature Reviews Neuroscience* **12**, 231–242 (2011).

41. R. A. Ozdemir, *et al.*, Individualized perturbation of the human connectome reveals reproducible biomarkers of network dynamics relevant to cognition. *Proceedings of the National Academy of Sciences* **117**, 8115–8125 (2020).

42. J. Wang, Y. He, Toward individualized connectomes of brain morphology. *Trends in Neurosciences* **47**, 106–119 (2024).

43. S. Zocher, *et al.*, Early-life environmental enrichment generates persistent individualized behavior in mice. *Science Advances* **6**, eabb1478 (2020).

44. M. Balerna, A. Ghosh, The details of past actions on a smartphone touchscreen are reflected by intrinsic sensorimotor dynamics. *npj Digital Med* **1**, 4 (2018).

45. R. L. Thorndike, Who belongs in the family? *Psychometrika* **18**, 267–276 (1953).

46. A. Delorme, S. Makeig, EEGLAB: an open source toolbox for analysis of single-trial EEG dynamics including independent component analysis. *Journal of Neuroscience Methods* **134**, 9–21 (2004).

47. L. Pion-Tonachini, K. Kreutz-Delgado, S. Makeig, ICLabel: An automated electroencephalographic independent component classifier, dataset, and website. *Neuroimage* **198**, 181–197 (2019).

48. D. Lehmann, W. Skrandies, Reference-free identification of components of checkerboard-evoked multichannel potential fields. *Electroencephalography and clinical neurophysiology* **48**, 609–621 (1980).

49. J. A. Palmer, K. Kreutz-Delgado, S. Makeig, AMICA: An adaptive mixture of independent component analyzers with shared components. *Swartz Center for Computatonal Neursoscience, University of California San Diego, Tech. Rep* 1–15 (2012).

50. J. A. Palmer, S. Makeig, K. Kreutz-Delgado, B. D. Rao, Newton method for the ICA mixture model in (IEEE, 2008), pp. 1805–1808.

51. A. Delorme, *et al.*, Research Article EEGLAB, SIFT, NFT, BCILAB, and ERICA: New Tools for Advanced EEG Processing. (2011).

52. D. D. Lee, H. S. Seung, Learning the parts of objects by non-negative matrix factorization. *Nature* **401**, 788–791 (1999).

53. E. Ceolini, A. Ghosh, Common multi-day rhythms in smartphone behavior. *npj Digit. Med.* **6**, 49 (2023).

54. P. A. Moran, Notes on continuous stochastic phenomena. *Biometrika* **37**, 17–23 (1950).

55. H. Li, C. A. Calder, N. Cressie, Beyond Moran's I: testing for spatial dependence based on the spatial autoregressive model. *Geographical analysis* **39**, 357–375 (2007).